Correlation between transport, dielectric, and optical properties of oxidized and nonoxidized porous silicon

B. Urbach, E. Axelrod, and A. Sa'ar*
Racah Institute of Physics and the Center for Nanoscience and Nanotechnology, the Hebrew University of Jerusalem, Jerusalem 91904, Israel

(Received 6 February 2006; revised manuscript received 11 April 2007; published 21 May 2007)

Using the correlation between transport, dielectric relaxation phenomena, and the state of oxidation of porous silicon, we have found that there are two major transport routes in the porous silicon medium. The first route of conduction via the disordered tissue that surrounds the silicon nanocrystals dominates for nonoxidized porous silicon and gradually disappears during the first stage of oxidation, where the disordered tissue is oxidized. The second route of tunneling and hopping in between the nanocrystals persists up to the second stage of oxidation where the nanocrystals are oxidized. This dual transport route model is consistent with the presence of two Meyer-Neldel rules and two power-law ac conductivities at mid and high temperatures. In addition, we have found that dc conduction is limited by narrow geometrical constrictions along the transport path that give rise to a Coulomb blockade type activation process. At lower temperatures the transport is characterized by a Cole-Cole relaxation associated with thermally activated intercrystallites hopping due to the shorter distances needed to walk by the carriers. Finally, for oxidized porous silicon we have found a new relaxation mechanism of interfacial polarization that is characterized by long relaxation times at high temperatures.

DOI: 10.1103/PhysRevB.75.205330 PACS number(s): 73.63.−b, 78.55.Mb, 77.22.Gm, 81.07.Bc

I. INTRODUCTION

Transport and conduction in structures containing nanoscale objects has been the subject of extensive research over the recent years.[1] In particular, silicon based nanostructures, such as porous silicon (PS),[2,3] have attracted considerable attention mainly due to the possibility of combining transport with the unique optical properties of PS.[4] While there is a general agreement that the optical properties of silicon based nanostructures, particularly the visible photoluminescence (PL),[5] should be connected with their nanoscale properties, there is much less knowledge and understanding how the local properties of silicon nanostructures contribute to transport phenomena. For example, in most cases luminescent PS is composed of a high porosity medium with fractal geometry, a surrounding disordered tissue and a distribution of small silicon nanocrystals (nc's)[6] which, all together can contribute to transport phenomena. The ability to distinguish between varieties of transport processes and to relate them to the nanoscale characteristics of the medium is a challenging topic that has not been fully addressed so far.

One of the experimental tools to link transport with nanoscale characteristics of PS is by studying the correlation between optical, structural and transport properties. This approach takes advantage of our current knowledge about these properties that can assign the variation in a specific property to a given component or a transport channel in the medium. Such an approach has been used recently by several groups to study the correlation between transport, structural properties and the PL from PS.[7,8] In this work, we extend this approach and investigate the correlation between transport, optical, structural properties and the state of oxidation of luminescent PS.[9–13] The integration of these techniques allows us not only to reveal the spectrum of transport and relaxation processes in PS, but also to identify the specific component of the PS medium that contributes to each transport channel. As a result, based on our findings, we can provide a comprehensive picture that relates transport phenomena to the structural properties of PS. We have found that there are two major transport routes in PS. The first route of conduction via the disordered tissue that surrounds the silicon nc's, dominates for nonoxidized PS and gradually disappear with oxidation as the tissue becomes less and less conductive. The second route of hopping in between the nc's dominates for oxidized PS. The existence of two transport routes is manifested by the presence of two Neldel-Meyer rules (NMRs)[14] in the dc conductivity and two power-law ac-conductivities [15–17] at mid and high temperatures with their relative contribution to the transport is in accordance with the state of oxidation. However, both transport routes are limited by narrow constrictions along the transport path that act as Coulomb blockade barriers. This finding explains the fairly large activation energies needed to activate dc conduction as compared to the characteristic energies for dielectric relaxation and ac conduction where the distance needed to walk by the carriers is much shorter, of the order of the distance between the nc's. The characteristic activation energies at low-temperatures, which are related to thermally activated intercrystallites hopping and characterized by a Cole-Cole relaxation form, are in accordance with the state of oxidation of the disordered tissue. Finally, at high temperatures and for oxidized PS, we have found a new, slow relaxation process that is related to a buildup of macroscopic interfacial polarization in the porous medium.

II. EXPERIMENT

PS samples were prepared by electrochemical anodization of 10–30 Ω cm, boron doped (100) *p*-type silicon wafers using a 1:1:2 $HF:H_2O:C_2H_5OH$ solution. Prior to anodiza-

TABLE I. Description of the fabrication processes for oxidized and nonoxidized PS samples.

Sample Process	Removal of the first backside Al contact	Oxidation time (s)	Second definition of Al backside contact
R	-	none	-
*t*0	+	0	+
*t*10	+	10	+
*t*20	+	20	+
*t*30	+	30	+
*t*60	+	60	+
*t*90	+	90	+
*t*150	+	150	+

tion a backside Al contact was evaporated and annealed at 460 °C for 20 min to form a good ohmic contact to the backside of the wafer. The anodization was carried out in the dark at a current density of 35 mA/cm^2 for 670 s. The PS thickness and porosity obtained by this process are ~20 μm and 75%, respectively.[17] We note that such a thick PS layer is necessary for our investigation as thin PS layers (of the order of a few microns or less) behave as a rectifying diode where the properties of the PS metal and the PS-silicon junctions dominate the transport.[18–20] As will be explained hereafter, for thick PS layers, we could verify that the measured electrical properties of the samples are related to the bulk PS medium rather than the contact junctions.

After anodization, the samples were rinsed in pentane and dried with nitrogen gas. Next, in order to thermally oxidize the PS samples we have performed the following steps. At first, the backside Al contact was removed by a mechanical polishing followed by cleaning of the samples. Next, the samples were oxidized in dry oxygen atmosphere, at a temperature of 900 °C, for different times that vary from 10 to 150 s (see Table I). After oxidation, new backside Al Ohmic contacts were evaporated and annealed (at 460 °C). Finally, 1-μm thick top Al contacts, 1 mm in diameter, were evaporated on top of the PS samples to form a metal/PS/silicon capacitor structure. In Table I we summarize the preparation conditions of the PS samples that are named according to their oxidation time. In addition, a reference PS sample (sample R in Table I) that was not oxidized and is similar to the sample studied in Refs. 16 and 17, has been prepared. Finally, for optical and infrared absorption measurements, we have prepared a set of similar samples, without a definition of top and backside metal contacts, so that PL and infrared transmission spectra could be measured using these samples.

Room temperature PL spectra were measured using the 488 nm line of Ar^+ ion laser as a source of excitation. The PL signal was dispersed by a 1/4 m monochromator, detected by a photomultiplier tube and analyzed by a photon counter. Infrared absorption spectra were measured using Fourier transform infrared (FTIR) spectrometer at room temperature.

For the dielectric spectroscopy, we have used a high resolution dielectric analyzer (NovoControl) that operates in the 0.1 Hz–1 MHz frequency range and in the 173–523 K temperature range. Measurements were done in the parallel plate capacitor configuration where the sample is placed in between two metal electrodes inside a vacuum cryosystem. At first, the sample was heated up to 423 K and held at that temperature for 6 h to remove any residual vapor from the sample. Next, the sample was cooled down to 173 K. Measurements were taken every 5 K over the entire temperature range. For dielectric response measurements the amplitude of a sinusoidal ac voltage source was kept constant at 1 V so that the average electric field across our samples is about 500 V/cm. For the thick PS samples used in our experiments, we could verify that the response is linear with respect to the ac voltage amplitude and that the effect of the contacts can be neglected so that a linear response analysis can be applied. In addition, for the analysis of the dc conductivity, the current-voltage (I-V) characteristics were measured in the −3 to 3 V range over the same temperature range.

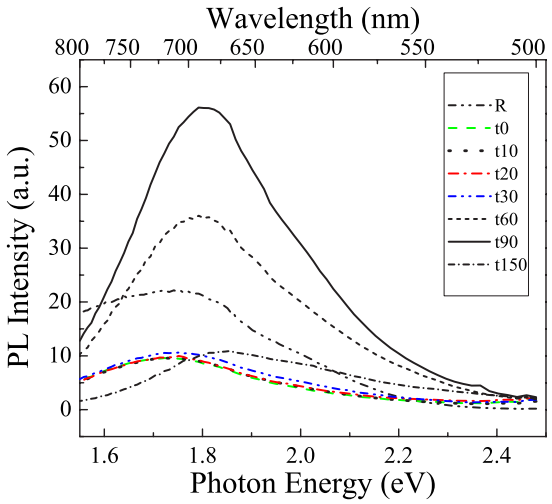

FIG. 1. (Color online) Room temperature PL spectra of the reference (R) and the oxidized PS samples.

III. RESULTS AND DATA ANALYSIS

A. PL and infrared absorption spectroscopy

Figure 1 presents the evolution of the PL spectra with the time of oxidation. One can see that up to 30 s of oxidation the PL spectrum is essentially unaffected by the oxidation showing a typical, fairly broad red PL emission centered at about ~1.7 eV.[2,3,11] In the range of 30–90 s time of oxidation, the PL spectrum increases in intensity and is blueshifted relative to nonoxidized PS. After 90 s of oxidation, the PL peak energy keep shifted to the blue, however, the PL intensity decreases rapidly with the time of oxidation. The above results are summarized in Fig. 2, where the variation of the PL peak energy [Fig. 2(a)] and the integrated PL intensity [e.g., the area below the PL spectra shown in Fig. 1; see Fig. 2(b)] versus the time of oxidation are presented and are in a good agreement with other reports on oxidation of PS.[9]

IR absorption spectra of oxidized and nonoxidized PS samples[21,22] are shown in Fig. 3. The spectra reveal several

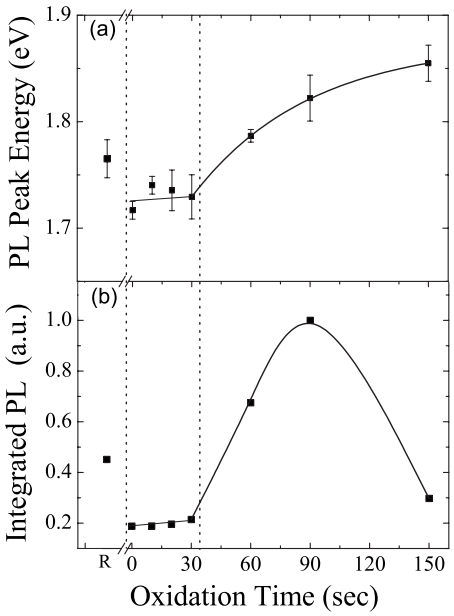

FIG. 2. The dependence of (a) the PL peak photon energy and (b) the integrated PL on the time of oxidation. The point R is related to the reference PS sample. The vertical dashed lines show the splitting into two stages of oxidation where the PL peak energy and the integrated PL are essentially constant during the first stage.

absorption bands that are related to Si-O-Si, Si-OH, O_n-SiH, and Si-H_n (n=1–3) modes of vibration. For the purpose of our investigation, we have chosen to follow the evolution of the Si-O-Si symmetric and asymmetric stretching modes at 812 cm^{-1} and at 1065–1190 cm^{-1}, respectively[23–25] and the Si-OH bending mode of vibration at 880 cm^{-1}.[26] We note that the Si-H_n stretching modes, at 2080–2140 cm^{-1},[27] disappear from the IR spectrum after alloying the contacts at 460 °C and therefore, are not suitable for tracing the state of

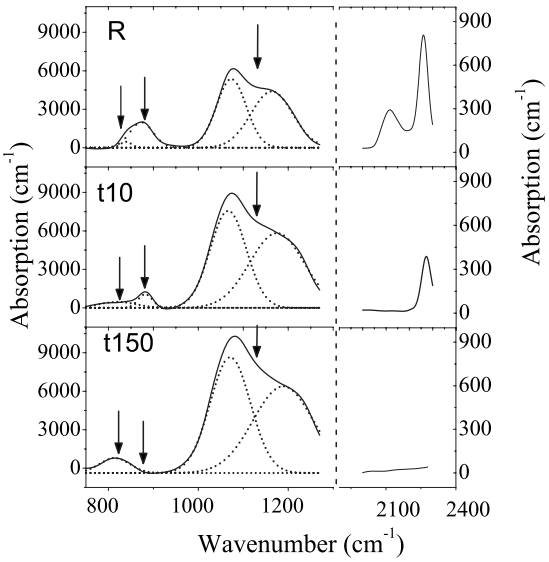

FIG. 3. Infrared absorption spectra of the reference PS (R) and the PS samples that were oxidized for 10 and 150 s. The arrows indicate the vibrational modes used to obtain Fig. 4 while the dashed lines represent Gaussian fitting of these modes.

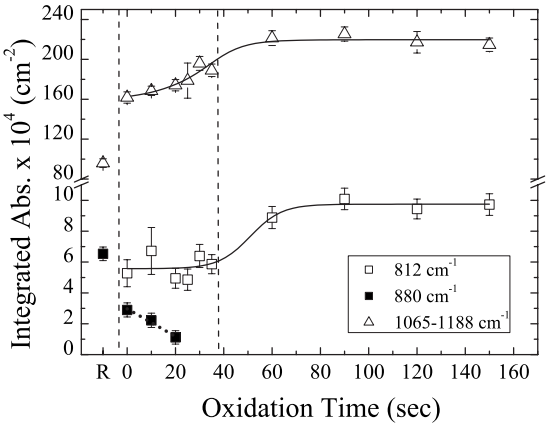

FIG. 4. The integrated IR absorption versus oxidation time for the various vibrational modes shown in Fig. 3. The empty symbols stand for the Si-O-Si modes of vibration while the full symbols stand for the Si-OH mode of vibration. Similar to Fig. 2, the vertical dashed lines represent a separation into two stages of oxidation.

oxidation of PS. The results, shown in Fig. 3, indicate that the amount of hydrogen in the PS medium decreases during the oxidation process until it cannot be observed after 30 s of oxidation. In order to quantify the amount of hydrogen/oxygen in our samples, we show in Fig. 4 the evolution of the integrated IR absorption (e.g., the area below each of the vibrational modes shown in Fig. 3) versus oxidation time. The amount of hydrogen that is bound to the PS matrix is traced by the area of the Si-OH bond at 880 cm^{-1}. It can be seen that this mode of vibration decreases very rapidly with the time of oxidation until it cannot be resolved after 30 s of oxidation. In addition, the O_n-SiH modes at 2240–2270 cm^{-1} also disappear after 20 s of oxidation, however, due to the low amplitude of these modes, they are not included in Fig. 4. On the other hand, both the 810 cm^{-1} and the 1070–1180 cm^{-1} silicon-oxygen modes of vibration show the same trend of increase up to ~60 s of oxidation and then, a saturation behavior indicating on a complete oxidation of the sample.

B. Dielectric spectroscopy

Results of dielectric spectroscopy for nonoxidized (R) and oxidized ($t30$ and $t150$) PS samples are presented in Fig. 5, where three-dimensional plots of the real (ε') and the imaginary (ε'') parts of the complex dielectric function $\varepsilon(\omega)=\varepsilon'-i\varepsilon''$, versus frequency and temperature are shown. Following the analysis described in Ref. 16, we define three temperature regimes where three distinct relaxation processes can be observed as follows.

Low temperatures process. This relaxation process, which extends over low temperatures (170–340 K), can be observed for nonoxidized samples and for samples that were oxidized up to about 30 s; see Fig. 5. For a given temperature of measurement, the process is characterized by a Cole-Cole (CC) relaxation function[28] given by[29].

$$\varepsilon(\omega) = \frac{\Delta\varepsilon}{1+(i\omega\tau)^{\alpha}}, \tag{1}$$

where $\Delta\varepsilon$ and τ are the amplitude and the relaxation time of the CC process, respectively, and α is the CC stretching ex-

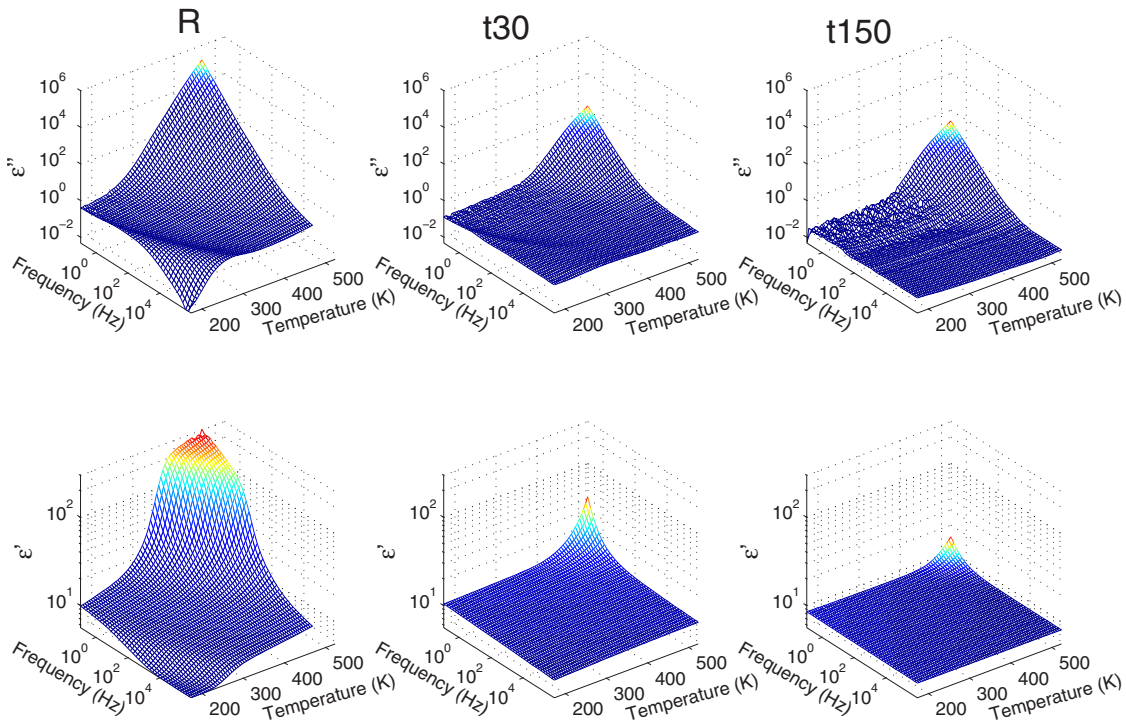

FIG. 5. (Color online) Three-dimensional plots of the imaginary part (top) and the real part (bottom) of the complex dielectric function versus frequency and temperature for (left) nonoxidized PS (sample R); PS samples that were oxidized for 30 s (middle) and 150 s (right), respectively.

ponent describing a deviation from a simple Debye relaxation (e.g., the case where $\alpha=1$).[30,31] The CC process is characterized by a temperature-dependent local maximum which, with the increasing time of oxidation, is shifted to higher frequencies until, after 30 s of oxidation its maximum frequency goes outside the measurement range of our dielectric spectrometer. In Fig. 6 we have plotted the amplitude of the CC process $\Delta\varepsilon$ versus temperature while in Fig. 7 we plot the CC relaxation times versus the inverse temperature for PS samples oxidized in the range of 0–30 s. All relaxation times, shown in Fig. 7, follow Arrhenius behavior of the form $\tau=\tau_0\exp(E_{CC}/kT)$, with E_{CC} being the activation energy of the process and τ_0 is the relaxation time prefactor.

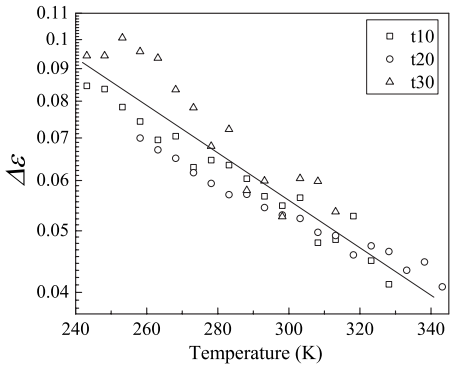

FIG. 6. The amplitude of the Cole-Cole relaxation process [see Eq. (1)] versus temperature for various oxidized PS samples. The solid line represents the exponential dependency of the amplitude on temperature, which is essentially independent on the time of oxidation.

Oxidation gives rise to smaller CC activation energies as can be seen from Figs. 7 and 8, where the relaxation time prefactors are plotted versus the activation energies. This behavior of the CC relaxation process will further be discussed in the next section.

Mid temperatures process. This relaxation process can be observed at low and mid temperatures (200–400 K). However, at low temperatures the CC process, discussed above, dominates over this process while at mid temperatures it becomes the dominant process in the dielectric spectrum.[16] The process can easily be observed for all oxidized samples; however, with the increasing time of oxidation the behavior of this process is gradually changed into a typical behavior of a dc-conductivity and should be analyzed as a part of the high-temperature process to be described in the next para-

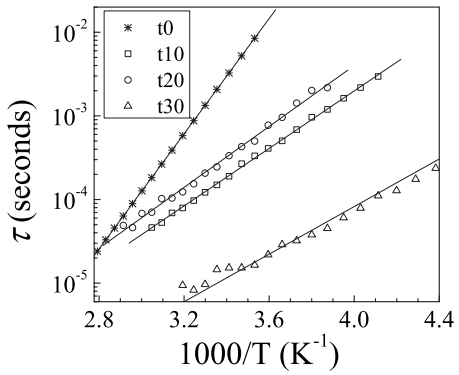

FIG. 7. Arrhenius Plot (semilog scale versus the inverse temperature) of the low temperature, Cole-Cole relaxation times of oxidized PS samples.

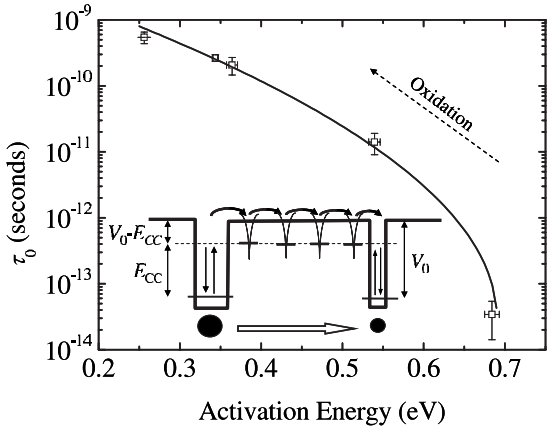

FIG. 8. Semilogarithmic plot of the CC relaxation time prefactors τ_0 versus the corresponding activation energies for a variety of oxidized and nonoxidized PS samples. The arrow indicates the direction of oxidation. The solid line represents the best fit to the data into Eq. (7). The inset schematically shows the model used to derive this equation.

graph. Following the analysis of Ref. 16, the mid-temperature complex dielectric function, at a given temperature of measurement, can be described as a superposition of two Jonscher terms[30] of the form

$$\varepsilon(\omega) = B_{\mathrm{LF}}(i\omega)^{n_{\mathrm{LF}}-1} + B_{\mathrm{HF}}(i\omega)^{n_{\mathrm{HF}}-1}. \quad (2)$$

Each of these Jonscher terms, that dominates at either low frequencies (the LF term) or at high frequencies (the HF term), describes a monotonic dependence of the dielectric function on frequency where B_{LF} (B_{HF}) and n_{LF} (n_{HF}) are the low (high) frequency Jonscher amplitude and exponent, respectively. Notice that $n=0$ describes a simple dc-conductivity term (e.g., $\varepsilon \sim 1/\omega$, so that $\sigma \sim \omega\varepsilon \sim$ const) while $n=1$ describes a simple dielectric medium without dispersion. In Fig. 9 we show the imaginary part of ε versus frequency, at 373 K, for various oxidation times. The dashed lines in this figure represent the two Jonscher terms that are extracted from fitting the experimental data to Eq. (2). While for nonoxidized PS and for samples with short oxidation

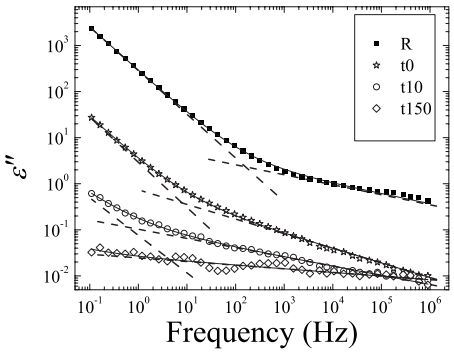

FIG. 9. Frequency dependence of the imaginary part of the complex dielectric function (ε'') at 373 K for oxidized and nonoxidized (sample R) PS samples. The solid lines represent the best fit of the data to Eq. (2) while the dashed lines represent a separate plot of the LF and the HF Jonscher terms for each sample.

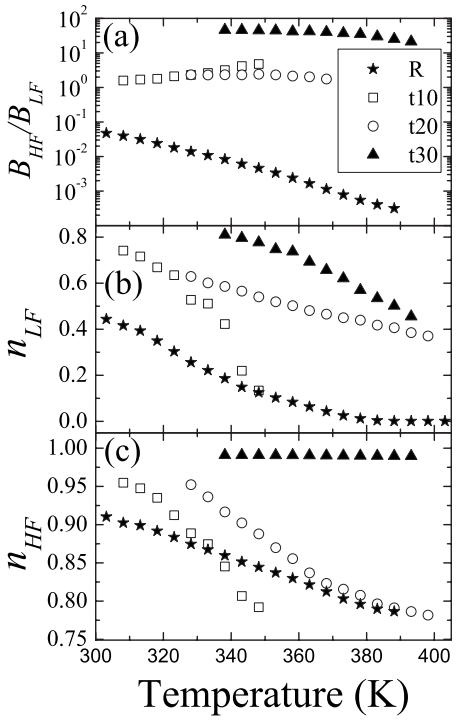

FIG. 10. (a) The ratio between the high-frequency (HF) and the low-frequency (LF) Jonscher amplitudes; (b) the LF Jonscher exponent, and (c) the HF Jonscher exponent versus temperatures for the reference and for oxidized PS samples.

times one can easily observe two Jonscher processes at low and high frequencies, for longer oxidation times only the high-frequency process can be observed. In order to quantify this behavior we show in Fig. 10(a) the ratio of the two Jonscher amplitudes $B_{\mathrm{HF}}/B_{\mathrm{LF}}$ versus temperature for various oxidation times. Notice that with the increase of the oxidation time, the HF process becomes the dominant process. In fact, after 30 s of oxidation, only the HF process could be resolved. In Figs. 10(b) and 10(c) we show the temperature dependence of the two Jonscher exponents for various oxidation times. Both the LF and the HF exponents decrease with the increasing temperature. However, while for nonoxidized PS and for short oxidation times ($t \leq 10$ s) the LF process gradually changes into a dc-conduction behavior, i.e., $n_{\mathrm{LF}} \rightarrow 0$ with the increasing temperature; for longer time of oxidation the LF process does not show a transition into a dc behavior and remains in the range of $n_{\mathrm{LF}} \sim 0.5-0.7$. On the other hand, the HF process, that dominates for highly oxidized PS samples, shows a pure dielectric behavior (e.g., $n_{\mathrm{HF}} \rightarrow 1$) for samples oxidized for 30 s or more.

High-temperature process. High-temperature relaxation processes can be observed for all PS samples, even those samples that were oxidized for the longest duration (see Fig. 5). The process is most significant at temperatures above 400 K and its amplitude decreases with the increasing frequency. One major contribution to high-temperature relaxation comes from a dc conductivity that cannot be ignored even for highly oxidized PS samples. Furthermore, the presence of dc-conductivity may screen other high-temperature processes and makes the analysis of high-temperature relax-

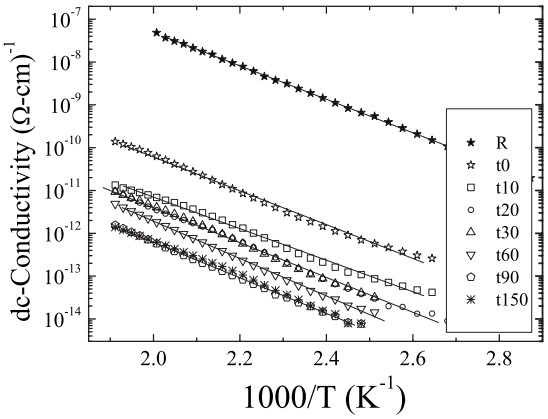

FIG. 11. Arrhenius plot of the dc-conductivity versus the inverse temperature for nonoxidized and oxidized PS samples. The solid lines represent fitting of the experimental data to a simple thermally activated process; see text.

ation phenomena a more difficult task. Hence, following the procedure described in Ref. 16, we first analyze the high-temperature dc conductivity of the PS samples and then subtract its contribution from the overall complex dielectric function to reveal additional high-temperature relaxation processes. We note that dc conductivity contributes only to the imaginary part of the complex dielectric function but not to its real part. Therefore, by applying the Kramers-Kronig relations[32] to the real part of the measured dielectric function $\varepsilon'(\omega)$ and subtracting the result from the imaginary part of the measured dielectric function $\varepsilon''(\omega)$ we find the difference between these two quantities to behave as follows:

$$\varepsilon''(\omega) - H[\varepsilon'(\omega)] = \frac{\sigma_{dc}}{\omega\varepsilon_0}, \tag{3}$$

where σ_{dc} is the dc conductivity and $H[\varepsilon'(\omega)]$ is the Hilbert transform of $\varepsilon'(\omega)$ (the mathematical transformation that correlates the real and the imaginary parts of a given analytical function via the Kramers-Kronig relations). In Ref. 16 we have shown that this differentiation is indeed vary as ω^{-1} as expected from our analysis. Similar results have been found in this work for all oxidized PS samples and have been verified by measurements of the *I-V* characteristics of the samples. Arrhenius plot of the dc conductivity versus the inverse temperature for oxidized and nonoxidized PS samples is shown in Fig. 11. The solid lines in this figure represent fitting of the experimental data to a simple thermally activated process $\sigma_{dc}=\sigma_0\exp(-E_{dc}/kT)$, where σ_0 is the dc-conductivity prefactor and E_{dc} is the activation energy of the dc conductivity. Further discussion of this behavior of the dc conductivity is given in the next section.

Next, after subtracting the background contribution of the dc conductivity from the measured dielectric response data, we could reveal a second high-temperature relaxation process. The results are shown in Fig. 12 for two different oxidation times. Both the real and the imaginary parts of the isothermal complex dielectric function are best described by the Cole-Davidson (CD) dispersion function[33] given by

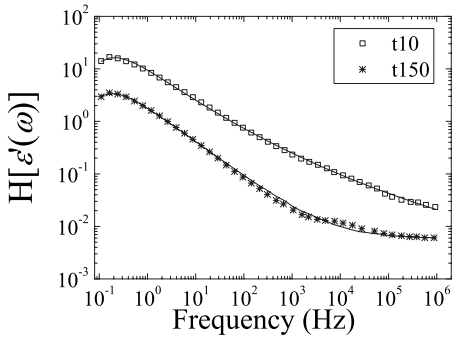

FIG. 12. Hilbert transform of the (measured) real part of the complex dielectric function at 523 K for oxidized PS samples. Notice that the data do not include the contribution of the dc conductivity. The solid lines represent the best fit to the Cole-Davidson expression (4).

$$\varepsilon(\omega) = \frac{\Delta\varepsilon}{(1+i\omega\tau)^{\beta}}, \tag{4}$$

where $\Delta\varepsilon$ and τ are the dielectric strength and the CD relaxation time, respectively, and β is the CD asymmetric broadening exponent ranging in between 0 and 1. The variation of the CD relaxation times with temperature is shown in Fig. 13 for various oxidized PS samples. We note that the results for the reference (nonoxidized) PS sample differ from those of the oxidized samples and are similar to those found in Ref. 16 for nonoxidized PS. These findings will be discussed in the next section.

IV. DISCUSSION

In order to understand the various transport and relaxation phenomena and their correlation with the optical properties of PS, let us point out that the PL spectra shown in Fig. 1, particularly the blueshift of the PL peak energy with oxidation time (see Fig. 2), provide a direct tool to identify a variation in the average size of the silicon nc's that are distributed in the PS medium. Our results are in a good agreement with those of Wolkin *et al.*[34] and others[35] who found that, for oxygen terminated silicon nc's, the PL peak energy is blueshifted with oxidation for relatively large nc's (due to increase of the energy bandgap of the nc's). For smaller nc's

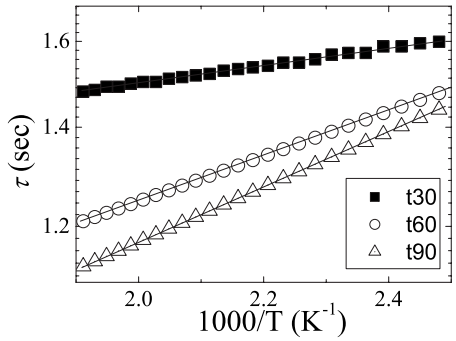

FIG. 13. The CD relaxation times versus the inverse temperature.

the energy bandgap of oxygen terminated silicon nc's is pinned due to the presence of localized states on the oxygen atoms,[36] which explains the saturation behavior of the PL peak energy; see Fig. 2. As a result, we can define two distinguishable oxidation regimes in our experiment. Up to 30 s of oxidation time, the silicon nc's are not affected by the oxidation process and neither a change in the PL intensity nor a PL blueshift have been observed. This conclusion is further supported by our IR absorption measurements, shown in Fig. 4, where the amount of hydrogen bonds rapidly decreases up to 30 s of oxidation time. Hence, we conclude that during the first 30 s of oxidation, the silicon nc's are not affected by the oxidation. Instead, the oxidation gives rise to a replacement of silicon-hydrogen bonds by silicon-oxygen bonds in the host disordered matrix of the PS medium, which is very likely composed of a mixture silicon skeletons with perturbed surface hydride bonds and amorphous silicon compounds such as hydrogenated amorphous silicon (a-Si:H), a-Si:OH, and SiO_x. After 30 s of oxidation all hydrogen terminated bonds disappear from the PS medium and the silicon nc's begin to oxidize as indicated by the blueshift of the PL peak energy during this stage of oxidation.

Let us discuss now the correlation between these findings and the dielectric properties of PS. At first, let us discuss the transport mechanism at mid temperatures where we have found that the dielectric response is characterized by LF and HF relaxation processes. We argue that the LF process takes place at the disordered tissue of the PS medium while the HF process should be associated with transport in between the silicon nc's. These conclusions are based on the fact that the amplitude of the LF process decreases very rapidly during the first stage of the oxidation and disappears after 30 s of oxidation; see Figs. 9 and 10(a). In contrast, the HF process persists up to the second stage of oxidation and becomes the dominant process among the two Jonscher-like transport processes. We emphasize that during the first stage of oxidation the nc's are not affected by the oxidation process (see Fig. 2) and therefore, the LF relaxation cannot be related to the nc's. On the other hand, the HF relaxation that becomes the dominant process after 30 s of oxidation cannot be associated with transport in the disordered tissue that surrounds the nc's as this tissue has already been oxidized after 30 s of oxidation (see Fig. 4). These experimental findings provide a direct support to models proposed by Ben-Chorin *et al.*[15] and by Balberg,[37] which argue that each of these transport channels should be linked with different components of the PS medium. Following these models we assign the LF process to a transport of carriers across the disordered fractal structure of PS. It has been shown by Ben-Chorin *et al.*[15] and by Lampin *et al.*[38] that, for such a transport channel the dielectric function should behave as $\varepsilon \sim \omega^{-1/2}$ (or $\sigma' \sim \omega^{1/2}$, where σ' is the real part of the ac conductivity), e.g., $n_{\mathrm{LF}} \cong 0.5$, as found in our experiment; see Fig. 10. Our findings assign this transport channel to the disordered tissue where, carriers located in shallow traps (impurity bonds) inside the tissue, within a range of kT from the Fermi edge, form a percolating network that is characterized by typical length scale of the order of the average size of the pores (10–100 nm in a typical PS). In nonoxidized PS, this process can be observed at mid temperatures, however, with the increasing temperature of measurement, dc conductivity takes over as the dominant relaxation process at low frequencies and screens the LF process as found in this work (see Fig. 10), in Ref. 16, and has been predicted by Ben-Chorin *et al.*[15] On the other hand, once the disordered tissue begins to oxidize (e.g., hydrogen bonds are replaced by oxygen bonds), fewer carriers are available for this conduction channel across the fractal structure. As a result, the amplitude of this process decreases until, after 30 s of oxidation, it completely disappears from the dielectric spectrum in a good agreement with our experimental findings.

Turning to the HF relaxation process, we conclude that this transport channel takes place in between the silicon nc's rather then the disordered tissue. At higher frequencies, the characteristic distance that the carriers can walk before the electric field changes its polarity becomes comparable to the average distance between the nc's (which is of the order of a few nm in a typical PS structure). As a result, a second process of intercrystallites hopping with fluctuating activation energies, appears in the dielectric spectrum. It has been shown[15] that this process should behave as, $\varepsilon \sim$ const (or $\sigma' \sim \omega$) meaning that, $n_{\mathrm{HF}} \cong 1$, in a good agreement with our experimental results shown in Fig. 10. Once oxidation begins, the HF process becomes more and more dominant. This result is consistent with our proposed picture as the intercrystallites distance should not be affected by the oxidation during the first stage of oxidation as the properties of the disordered tissue are less relevant to this transport channel. Furthermore, during oxidation, the amplitude of the LF process decreases and the HF process becomes the only available transport channel at mid temperatures. As a result, after 30 s of oxidation, the HF exponent n_{HF} approaches a value close to 1 (within the experimental error) as shown in Fig. 10(c) and predicted by the model of Ben Chorin *et al.*[15] Hence, our experimental results seem to confirm this model and the theoretical predictions related to this range of temperatures.

A very similar picture, of two transport routes, is obtained for the dc conductivity. We would like to emphasize that the dc conductivity in our relatively thick PS samples could not be measured at low and mid temperatures, neither by dielectric spectroscopy nor by direct IV measurements. On the other hand, at high temperatures, dc conductivity has been observed even for highly oxidized PS samples. In this respect, our PS samples differ from fully oxidized PS (that can be considered as a simple porous glass) where the dc conductivity and the PL diminish (since all silicon nc's are fully oxidized). The dc conductivity of our samples follows a simple Arrhenius behavior $\sigma_{\mathrm{dc}} = \sigma_0 \exp(-E_{\mathrm{dc}}/kT)$, where the activation energies and the conductivity prefactors (E_{dc} and σ_0, respectively) are extracted by the fitting to the solid lines shown in Fig. 11. Here, we have found a fundamental distinction between all oxidized samples (including sample $t0$) and the reference, nonoxidized PS sample (sample R). While the activation energy of *all* samples, including the reference PS, are essentially the same, equal to ~0.85 eV independent on the state of oxidation, the dc conductivity prefactors of the reference PS sample substantially differs from those of the oxidized samples. This is shown in Fig. 14, where both the activation energies and the dc-conductivity prefactors are

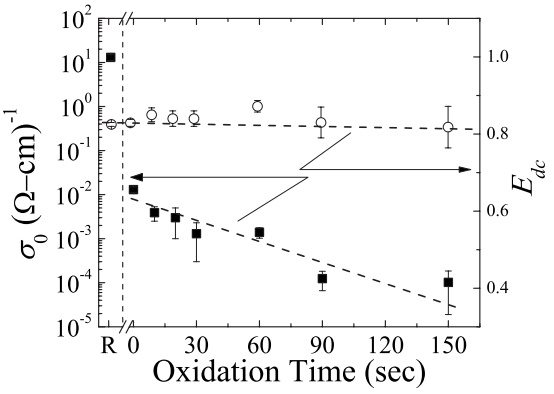

FIG. 14. The experimental values of the dc-conductivity prefactors (■) and the corresponding activation energies (○) versus the oxidation time. The dashed lines represent the second MNR for all oxidized PS samples (including sample *t*0) while the notation R stands for the reference PS with a conductivity prefactor that is three orders of magnitude larger (first MNR).

plotted versus the oxidation time. While σ_0 of the oxidized samples is in the range of 10^{-2}–10^{-4} Ω^{-1} cm^{-1}, the conductivity prefactor of the reference, nonoxidized PS is more than three orders of magnitude larger ~ 10 Ω^{-1} cm^{-1}; see Fig. 14. This result indicates that the transport mechanism associated with the nonoxidized sample differs from that responsible to the dc conductivity of the oxidized samples. Such a dual transport picture has been proposed in Refs. 14 and 37 and has been assigned to the presence of two Meyer-Neldel-Rules (MNR)[39,40] in PS. Each of these rules is related to a specific transport mechanism that can coexist with the other in the PS medium. Our experimental results support this picture. Following the pea-pod model of Ref. 37 we assign the first transport channel, which takes place in the nonoxidized PS sample (sample R), to extended states transport in the conductive, disordered tissue of the PS medium. However, after a short time of oxidation (in fact, even after alloying the contacts at 460 °C), a second transport channel of intercrystallites hopping, which is related to a second MNR, takes over. Our results provide a support to the assumption that the second MNR is associated with transport in between the silicon nc's, as this channel of transport persists well into the second stage of oxidation. In addition, our experimental results indicate that the activation energy associated with the dc conductivity has a very weak dependency on the oxidation process; see Fig. 14. Similar phenomenon, e.g., activation energy of the dc conductivity that is not affected by the oxidation despite that the transport mechanism is changed from the first MNR (conduction in the disordered tissue) to a second MNR (intercrystallites hopping), has also been observed by other groups.[20] This result indicates that the activation energy, associated with the dc conductivity in a given PS sample, should be independent on the choice of a specific transport channel (e.g., the MNR) neither on the state of oxidation. For example, if a geometrical factor such as geometrical constrictions along both transport channels is responsible for this activation energy, one could explain the above experimental findings by this model. Such a model of surface/geometrical constrictions along the conduction paths has been proposed by Lehmann *et al.*[41] for explaining the high resistance of meso-PS. These constrictions, which simultaneously affect conduction paths along both the disordered tissue and in between the nc's, trap charged carriers. As a result, the trapped charges block the transport channels by their electric field. It has been estimated that constrictions as narrow as 10 nm (or less) could cause to a partial blocking of the current path in relatively thin PS layers.[41] These constrictions can be viewed as Coulomb blockade centers[42] that require additional thermal activation of the carriers for passing through them. We emphasize that this picture does not contradict the pea-pod model[37] neither the distribution of activation energies found in Ref. 14, as different PS samples are characterized by different geometries, length scales and other statistical parameters that determine the specific value of the activation energy. Furthermore, such constrictions are expected to influence both channels of dc-conduction as the geometry of the PS medium is essentially independent on the state of oxidation. Let us also point out that our model is consistent with recent experiments where the *I-V* characteristics of relatively thin PS layers at low temperatures have been found to be dominated by the Coulomb blockade mechanism.[42]

Up to now, all transport phenomena discussed so far (e.g., dc and ac conductivities at mid and high temperatures) seem to consistently follow the dual transport route model. Let us turn now to the low-temperature CC relaxation process, which requires a more careful analysis in view of this model. Here, we argue that this relaxation process takes place in between the silicon nc's. This conclusion is based on the results shown in Fig. 6, where the amplitude of the CC relaxation process has been found to be essentially independent on the time of oxidation during the first stage of oxidation. On the other hand, the CC relaxation times and, in particular, the CC activation energies show a considerable dependency on the state of oxidation during the first stage of oxidation (see Figs. 7 and 8). We also notice that the CC relaxation cannot be considered as a simple mobility edge hopping[43] via extended states or via band tails as in the case of dc conduction as this is a thermally activated process of the form $\tau^{-1}=\tau_0^{-1}\exp(-E_{CC}/kT)$. Therefore, we suggest that the CC process is related to a thermally activated tunneling and hopping in between silicon nc's via localized states located in the disordered tissue that wrap the nc's. A simple, semiquantitative model of sequential tunneling in between adjacent nc's, is presented at the inset to Fig. 8. In this model, carriers (most likely, holes[16]) in the nc's are thermally excited into a higher excited state located at (average) energy, E_{CC}, above the ground state. This activation energy, which allows hopping of thermally excited carriers via shallow traps in the surrounding tissue, is determined by those traps located in the disordered tissue. Hence, modeling the nc's by a simple rectangular well with a potential energy V_0 (where we have neglected the external voltage drop across the barrier that is expected to be much smaller compared to V_0) then, the additional barrier energy that the carriers should tunnel through is $\sim(V_0-E_{CC})$. Accordingly, the tunneling probability T can be approximated as follows:

$$T \sim e^{-2L\sqrt{2m_2(V_0-E_{CC})}/\hbar}, \tag{5}$$

where m_1 and m_2 are the holes effective masses in the nc's and in the barriers and d and L are the average sizes of the nc's and the tunnel barriers respectively. Therefore, the tunneling time in between the nc's can be estimated as follows:

$$\frac{1}{\tau_0} = \frac{\sqrt{2E_{CC}/m_1}}{2d} T(E_{CC}) \sim e^{-2L\sqrt{2m_2(V_0-E_{CC})}/\hbar}. \tag{6}$$

From this simple model of thermally activated hopping we find that $\ln \tau_0 \cong K\sqrt{V_0 - E_{CC}}$, where K is a constant that depends on the masses and the geometry of the system. The solid line in Fig. 8 represents a fitting of the experimental data to the above model of thermally activated hopping in between the silicon nc's. From the fitting we find $V_0 \cong 0.69 \pm 0.01$ eV. This potential energy is expected to be smaller than the activation energy for dc conduction (~0.85 eV, see Fig. 14) as the distance walked by the carriers before the electric field changes its polarity is smaller than the average distance between constrictions. We would like to emphasize that our simplified model ignores details of the hopping process in the surrounding tissue. The influence of the tissue on the hopping process has been taken into account by setting up the activation energy E_{CC} according to the (relative) energy of the impurity states in the surrounding tissue. Yet, the effect of oxidation on the CC activation energies and the relaxation time prefactors has been found to be consistent with this picture. For nonoxidized PS the measured activation energy is about ~0.68 eV (very close to V_0; see Fig. 8) meaning that the impurity states in the disordered tissue behave as shallow traps giving rise to a fairly good conduction of this tissue. Oxidation gives rise to a decrease of E_{CC} (see Fig. 8) meaning that these traps become more profound and localized in the surrounding tissue[44–46]that, in turn, becomes less conductive. This mechanism gives rise to a simple relation between the relaxation time prefactors and the activation energies as follows:

$$\tau_0 = \tau_{0,CC} \exp(K\sqrt{V_0 - E_{CC}}), \tag{7}$$

where $\tau_{0,CC}$ is the relaxation time prefactor of the conductive (nonoxidized) tissue (e.g., $E_{CC} \approx V_0$). This is also the expression used for the fitting (solid line) shown in Fig. 8.

Finally, let us discuss the origin of the high-temperature CD relaxation process; see Fig. 13. We would like to point out that the CD process in all oxidized PS samples is characterized by fairly slow relaxation times, of the order of few seconds, and a weak dependency on temperature. Such slow relaxation times and temperature dependencies exclude the possibility that the CD process can be linked to a simple electronic transport via the nc's (this process cannot be associated with a transport in the disordered tissue as the process persists up to the second stage of oxidation where the disordered tissue has already been oxidized). A similar dielectric behavior, with very slow relaxation times of the order of few milliseconds up to few seconds, has been found in other porous insulating matrices such as borosilicate glasses.[47,48] In those porous insulators, the appearance of slow relaxation times and small activation energies has been attributed to interfacial polarization created at the interface of the host matrix and the walls of the pores.[47] We assign the high temperature CD relaxation process in the oxidized PS samples to a similar phenomenon where thermally activated charged carriers, which can hope in between the nanocrystals (see the second MNR of intercrystallites hopping), are trapped at the host matrix-air interface. Such a process gives rise to a buildup of a space charge polarization field that is characterized by a macroscopically large charge separation. This mechanism of interfacial polarization provides a simple explanation to the appearance of long relaxation times that are required to activate the macroscopic interfacial polarization. The process dominates at high temperatures where a sufficient number of thermally activated carriers are available to construct the interfacial polarization. However, the relaxation times associated with this process have a weak dependency on temperature as the activation of the interfacial polarization is determined mainly by the fractal geometry of the pores and the (oxidized) host matrix. Our model is consistent with a recent observation of slow luminescence decay times from oxidized PS, of the order of few seconds, which were also assigned to trapped charges in oxidized PS.[49] Also, other models for PL from silicon nc's embedded in PS and in SiO_2 emphasize the role of oxygen traps.[11,50,51] Following these findings, we can now provide a simple explanation to the high temperature relaxation process that appears in nonoxidized PS. In Ref. 16 we have found that in nonoxidized PS the high-temperature relaxation process is characterized by a multiple Arrhenius behavior (or other, more complicated fitting functions). Based on the current analysis, we suggest that the multiple Arrhenius behavior of nonoxidized PS should be assigned, again, to interfacial polarization. However, as opposed to oxidized samples, in nonoxidized PS the interfacial polarization can be constructed via both hopping in between the nanocrystals as well conduction along the disordered tissue. Both channels of conduction are allowed in nonoxidized PS and contribute to trapping of charged carriers at the host matrix-air interface. It is the contribution of both transport channels to interfacial polarization that makes the high-temperature relaxation process in nonoxidized PS, a more complicated process with multi-Arrhenius behavior as found in our experiments and in Ref. 16.

V. CONCLUSIONS

To conclude the main findings of this work, let us discuss a comprehensive picture that summarizes the various transport phenomena in PS; see Fig. 15. In principle, there are two transport routes that are related to the two basic components of the PS medium. These are the disordered tissue that surrounds and wraps the nc's and the nc's themselves. In nonoxidized PS both components of the PS medium contribute simultaneously to the transport. For example, both the LF and the HF relaxation processes coexist in the (nonoxidized) PS medium at mid temperatures. During oxidation there are two stages that affect both the transport and the PL from the PS medium. At the first stage of oxidation, the disordered tissue is oxidized and silicon-hydrogen bonds are replaced by silicon-oxygen bonds. During this stage, the transport

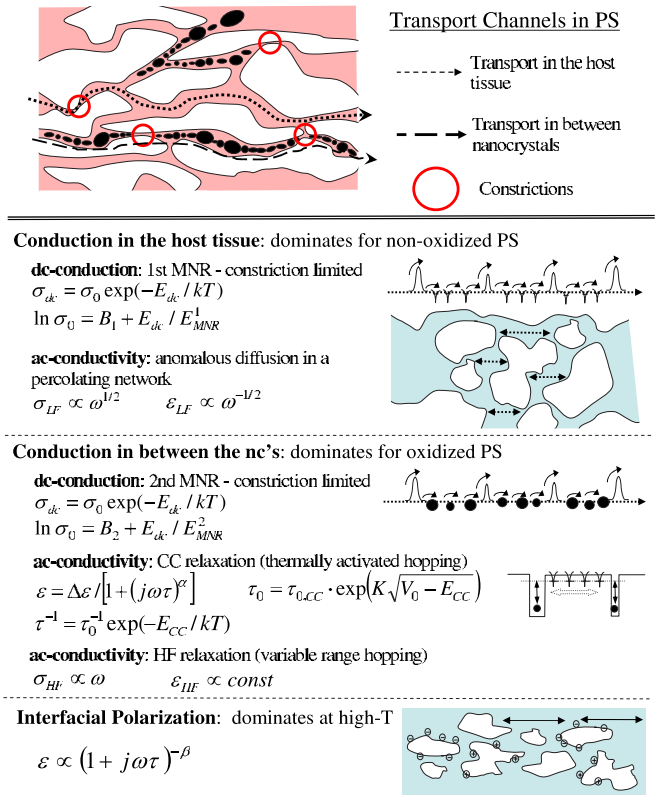

FIG. 15. (Color online) Schematic illustration and summary of the various transport channels in PS. The dashed line represents transport routes in the disordered tissue including dc conduction via narrow constrictions (first MNR) and anomalous ac conduction (LF process). The bold dash line represents transport channels associated with hopping in between the nc's. The red open circles stand for geometrical constrictions along the transport path for both cases.

channels that take place in the disordered tissue are gradually blocked and eventually disappear from the dielectric response spectrum. This includes the LF relaxation process and the dc conductivity associated with the first MNR. All other transport channels that are related to hopping in between the silicon nc's are not affected at this stage of oxidation. During the second stage of oxidation only those channels that are related to intercrystallites transport persist. This includes the CC relaxation, the HF process and the second MNR that is related to dc conduction. Our model also provides a simple explanation to the relatively large energies required to activate dc conduction that are due to narrow geometrical constrictions along the transport path that act as Coulomb blockade barriers. On the other hand, the energies required for activating the CC relaxation and the ac conduction are considerably smaller as the distances walked by the carriers are much shorter. Finally, at high temperatures there is another relaxation process of interfacial polarization that is related to a space charge polarization buildup at the interface of the pore's walls. This process is similar to relaxation processes observed in other porous glasses and is not related directly to the silicon nc's but rather to the mechanism that generates the macroscopic space charge polarization on the walls of the pores.

Our last comment is related to the expressions used to describe the CC and the CD relaxation processes; see Eqs. (1) and (4) respectively. In the literature there is a very limited discussion about the physical mechanisms that are responsible to the appearance of either expression.[52] Our findings suggest that the CC relaxation process is associated with local interactions such as the dipole-dipole interactions. In PS this is related to intercrystallites hopping for which the CC process seems to provide the best description. On the other hand, the CD mechanism should be assigned to interaction of the local dipoles with the host matrix, as in the case of interfacial polarization found in our PS media. However, the universality of this rule has to be experimentally investigated in other materials systems and to be verified theoretically. These topics are behind the scope of this work.

ACKNOWLEDGMENTS

The authors express their sincere gratitude to I. Balberg and Y. Feldman for a critical reading of the manuscript and for valuable discussions. This work was supported by Grant No. 422/04 of the Israel Science Foundation (ISF) and by the Israeli Ministry of Science. One of us (E.A.) acknowledges the Israeli Ministry of Science for financial support. We thank the technical staff of the Unit for Nano-Characterization (UNC) at the Hebrew University of Jerusalem for their technical support.

*Email address: saar@vms.huji.ac.il

[1] D. K. Ferry and S. M. Goodnick, *Transport in Nanostructures*, (Cambridge University Press, Cambridge, 1997); *Single-Charge Tunneling*, edited by H. Grabet and M. H. Devoret (Plenum, New York, 1992).

[2] A. G. Cullis, L. T. Canham, and P. D. J. Calcott, J. Appl. Phys. **82**, 909 (1997).

[3] For a collection of reviews see, *Light Emission in Silicon: From Physics to Devices*, edited by D. J. Lockwood (Academic, New York, 1998); W. Theiß, Surf. Sci. Rep. **29**, 91 (1997); O. Bisi, S. Ossicini, and L. Pavesi, *ibid.* **38**, 1 (2000); L. Pavesi, L. Dal Negro, C. Mazzoleni, G. Franzo, and F. Priolo, Nature (London) **408**, 440 (2000).

[4] N. Koshida and N. Matsumoto, Mater. Sci. Eng., R. **40**, 169 (2003); L. Pavesi, C. Mazzoleni, A. Tredicucci, and V. Pellegrini, Appl. Phys. Lett. **67**, 3280 (1995).

[5] L. T. Canham, Appl. Phys. Lett. **57**, 1046 (1990).

[6] P. D. J. Calcott, K. J. Nash, L. T. Canham, M. J. Kane and D. Brumhead, J. Phys.: Condens. Matter **5**, L91 (1993); R. Shinar, D. S. Robinson, J. Partee, P. A. Lane, and J. Shinar, J. Appl. Phys. **77**, 3403 (1995).

[7] M. L. Ciurea, M. Draghici, V. Iancu, M. Reshotko, and I. Balberg, J. Lumin. **102**, 492 (2003).

[8] T. Ozaki, T. Oguro, H. Koyama, and N. Koshida, Jpn. J. Appl. Phys., Part 1 **34**, 946 (1995); B. Garrido, M. Lopez, O. Gonzales, A. Peres-Rodriguez, J. R. Morante, and C. Bonafos, Appl. Phys. Lett. **77**, 3143 (2000).

[9] K.-H. Li, C. Tsai, J. C. Campbell, B. K. Hance, and J. M. White, Appl. Phys. Lett. **62**, 3501 (1993); V. Petrova-Koch, T. Muschik, A. Kux, B. K. Meyer, and F. Koch, *ibid.* **61**, 943 (1992).

[10] Th. Dittrich, H. Flietner, V. Yu. Timoshenko, and P. K. Kashkarov, Thin Solid Films **255**, 149 (1995); R. R. Koropecki, R. D. Arce, and J. A. Schmidt, Phys. Rev. B **69**, 205317 (2004); L. Z. Zhang, B. Q. Zong, B. R. Zahng, Z. H. Xu, J. Q. Li, and G. G. Qin, J. Phys.: Condens. Matter **7**, 697 (1995).

[11] M. V. Wolkin, J. Jorne, P. M. Fauchet, G. Allan, and C. Delerue, Phys. Rev. Lett. **82**, 197 (1999).

[12] E. A. Petrova, K. N. Bogoslovskaya, L. A. Blagurov, and G. I. Kochordaze, Mater. Sci. Eng., B **69-70**, 152 (2000); J. M. Lauerhaas and M. J. Sailor, Science **261**, 1567 (1993); A. E. Pap, K. Kordas, G. Toth, J. Levoska, A. Uusimaki, and T. F. George, Appl. Phys. Lett. **86**, 041501 (2005).

[13] T. Ito, T. Ohta, O. Arakaki, and A. Hiraki, in *Light Emission from Silicon*, edited by Subramanian S. Iyer, Reuben T. Collins, and Leigh T. Canham, MRS Symp. Proc. No. 256 (Materials Research Society, Pittsburgh, 1992), p. 127; V. Lehmann, H. Cerva, and U. Goesele, *ibid.* **256**, 3 (1992); P. O'Keeffe, Y. Aoyagi, S. Komuro, T. Kato, and T. Morikawa, Appl. Phys. Lett. **66**, 836 (1995).

[14] Y. Lubianiker and I. Balberg, Phys. Rev. Lett. **78**, 2433 (1997).

[15] M. Ben-Chorin, F. Moller, F. Koch, W. Schirmacher, and M. Eberhard, Phys. Rev. B **51**, 2199 (1995).

[16] E. Axelrod, A. Givant, J. Shappir, Y. Feldman, and A. Sa'ar, Phys. Rev. B **65**, 165429 (2002).

[17] E. Axelrod, A. Givant, J. Shappir, Y. Feldman, and A. Sa'ar, J. Non-Cryst. Solids **305**, 235 (2002); E. Axelrod, B. Urbach, A. Sa'ar, and Y. Feldman, J. Phys. D **39**, 16 (2006).

[18] S. Pilla, B. Naberhuis, and J. Goodkind, J. Appl. Phys. **98**, 024508 (2005).

[19] M. Theodoropoulou, C. A. Krontiras, N. Xanthopoulos, S. N. Georga, M. N. Pisanias, C. Tsamis, and A. G. Nassiopoulou, Mater. Sci. Eng., B **101**, 334 (2003).

[20] D. G. Yarkin, L. A. Balagurov, S. C. Bayliss, and I. P. Zvyagin, Semicond. Sci. Technol. **19**, 100 (2004).

[21] W. Theiss, S. Hilbrich, R. Arens, M. G. Berger, and H. Hunter, in *Structural and Optical Properties of Porous Silicon Nanostructures*, edited by G. Amato, C. Delerue, and H. J. von Bardeleben (Gordon and Breach, New York, 1997); M. S. Brandt, H. D. Fuch, M. Stutzmann, J. Weber, and M. Cardona, Solid State Commun. **81**, 307 (1992); V. M. Dubin, F. Ozanam, and J.-N. Chazalviel, Vib. Spectrosc. **8**, 159 (1995).

[22] K.-H. Li, D. C. Diaz, and J. C. Campbell, in *Porous Silicon*, edited by Z. C. Feng and R. Tsu (World Scientific, Singapore, 1994), pp. 261–274.

[23] P. Li, G. Wang, Y. Ma, and R. Fang, Phys. Rev. B **58**, 4057 (1998).

[24] C. T. Kirk, Phys. Rev. B **38**, 1255 (1988).

[25] A. Borghesi, A. Sassella, B. Pivac, and L. Pavesi, Solid State Commun. **87**, 1 (1993).

[26] K. M. Davis and M. Tomozawa, J. Non-Cryst. Solids **201**, 177 (1996).

[27] V. M. Dubin, F. Ozanam, and J. N. Chazalviel, Thin Solid Films **255**, 87 (1995).

[28] The CC form is a simplified version of the more general Harviliak-Negami relaxation form that has been found to better describe low-temperature relaxations in PS (see Ref. 16).

[29] K. S. Cole and R. H. Cole, J. Chem. Phys. **9**, 341 (1941).

[30] A. K. Jonscher, *Universal Relaxation Law* (Chelsea Dielectric Press, London, 1983); J. C. Dyre and T. B. Schroeder, Rev. Mod. Phys. **72**, 873 (2000); Y. Feldman, A. Puzenko, and Y. Ryabov, Chem. Phys. **284**, 139 (2002).

[31] A. K. Jonscher, *Dielectric Relaxation in Solids* (Chelsea Dielectric Press, London, 1996).

[32] C. J. F. Böttcher and P. Bordewijk, *Theory of Electric Polarization* (Elsevier Science, Amsterdam 1992).

[33] D. W. Davidson and R. H. Cole, J. Chem. Phys. **19**, 1484 (1951).

[34] M. V. Wolkin, J. Jorne, P. M. Fauchet, G. Allan, and C. Delerue, Phys. Rev. Lett. **82**, 197 (1999).

[35] S. Schuppler, S. L. Friedman, M. A. Marcus, D. L. Adler, Y.-H. Xie, F. M. Ross, Y. J. Chabal, T. D. Harris, L. E. Brus, W. L. Brown, E. E. Chaban, P. F. Szajowski, S. B. Christman, and P. H. Citrin, Phys. Rev. B **52**, 4910 (1995); L. Z. Zhang, B. Q. Zong, B. R. Zahng, Z. H. Xu, J. Q. Li, and G. G. Qin, J. Phys.: Condens. Matter **7**, 697 (1995).

[36] G. Allan, C. Delerue, and M. Lannoo, Phys. Rev. Lett. **76**, 2961 (1996); M. Luppi and S. Ossicini, Phys. Rev. B **71**, 035340 (2005); I. Vasiliev, J. R. Chelikowsky, and R. M. Martin, *ibid.* **65**, 121302(R) (2002); M. Nishida, *ibid.* **69**, 165324 (2004).

[37] I. Balberg, Philos. Mag. B **80**, 691 (2000).

[38] E. Lampin, C. Delerue, M. Lannoo, and G. Allan, Phys. Rev. B **58**, 12044 (1998).

[39] H. Oeverhof and P. Thomas, *Electric Transport in Hydrogenated Amorphous Semiconductors* (Springer-Verlag, Berlin, 1989).

[40] J. C. Dyre, J. Phys. C **19**, 5655 (1986).

[41] V. Lehmann, F. Hofmann, F. Moller, and U. Gruning, Thin Solid Films **255**, 20 (1995).

[42] M. R. Reshotko, A. Sa'ar, and I. Balberg, Phys. Status Solidi A **197**, 113 (2003); A. Deligenti, A. Nannini, G. Pennneli, and F. Pieri, Appl. Phys. Lett. **68**, 687 (1996); N. Lalic and J. Linnros, J. Appl. Phys. **80**, 5971 (1996); B. Hamilton, J. Jacobs, D. A. Hill, R. F. Fettifer, D. Teehan, and L. T. Canham, Nature (London) **393**, 443 (1998).

[43] L. Burstein, Y. Shapira, J. Partee, J. Shinar, Y. Lubianiker, and I. Balberg, Phys. Rev. B **55**, R1930 (1997).

[44] A. Janotta, R. Janssen, M. Schmitt, T. Graf, L. Görgens, C. Hammerl, S. Schreiber, G. Dollinger, A. Bergmaier, B. Stritzker, and M. Stutzmann, J. Non-Cryst. Solids **299-302**, 579 (2002).

[45] A. Bacioglu, A. O. Kodolbas, and O. Oktu, J. Mater. Sci.: Mater. Electron. **14**, 737 (2003).

[46] D. Das and A. K. Barua, Sol. Energy Mater. Sol. Cells **60**, 167 (2000).

[47] A. Gutina, T. Antropova, E. Rysiakiewicz-Pasek, K. Virnik, and Y. Feldman, Microporous Mesoporous Mater. **58**, 237 (2003).

[48] A. Gutina, E. Axelrod, A. Puzenko, E. Rysiakiewicz-Pase, N. Kozlovich, and Y. Feldman, J. Non-Cryst. Solids **235**, 302 (1998).

[49] A. Kux, D. Kovalev, and F. Koch, Thin Solid Films **255**, 143 (1995).

[50] M. Dovrat, Y. Goshen, J. Jedrzejewsky, I. Balberg, and A. Sa'ar, Phys. Rev. B **69**, 155311 (2004); M. Dovrat, Y. Goshen, I. Popov, J. Jedrzejewski, I. Balberg, and A. Sa'ar, Phys. Status Solidi C **2**, 3440 (2005).

[51] A. Sa'ar, Y. Reichman, M. Dovrat, D. Krapf, J. Jedrzejewsky, and I. Balberg, Nano Lett. **5**, 2443 (2005); A. Sa'ar, M. Dovrat, J. Jedrzejewsky, and I. Balberg, Physica E (Amsterdam) **38**, 122 (2007); A. Sa'ar, M. Dovrat, J. Jedrzejewski, I. Popov, and I. Balberg, Phys. Status Solidi A **204**, 1491 (2007).

[52] R. R. Nigmatullin and Ya. E. Ryabov, Phys. Solid State **39**, 87 (1997); Ya. E. Ryabov and Y. Feldman, Fractals **11**, 173 (2003).